PROCEEDINGS, Thirty-Fifth Workshop on Geothermal Reservoir Engineering
Stanford University, Stanford, California, February 1-3, 2010
SGP-TR-188

SIMULATION OF FLUID FLOW IN FRACTURED PORO-THERMOELASTIC RESERVOIRS

Qingfeng Tao and Ahmad Ghassemi

Texas A&M University
College Station, TX 77054, USA
e-mail: ahmad.ghassemi@pe.tamu.edu

ABSTRACT

This paper examines the problem of injection/extraction into a naturally fractured rock by considering the role of poro-thermoelastic processes and joint deformation on reservoir permeability change and fracture pressure variation. This is accomplished by considering fluid flow and heat transport in a 2D model of a fracture network that is based on the displacement discontinuity technique. It is assumed that the fracture aperture and joint deformation are significantly less than the joint lengths, there are a large but finite number of joints, and fluid in the fractures is compressible. The total normal stress in the direction normal to the joint varies non-linearly but, in the shear direction the joint stresses are proportional to deformation when the deformation are in the elastic range, and the joint dilation is considered. Numerical experiments are presented to illustrate the role of poro-thermoelatic effects as well as joint constitutive behavior on the reservoir response to injection and extraction.

INTRODUCTION

Design of enhanced geothermal system (EGS) can benefit from simulation of coupled rock deformation and fluid flow in fractured reservoirs where there exist coupled interactions among fluid and heat flow, and mechanical response of the fracture and matrix. The full coupling between these processes can be modeled using the linear theory of poro-themoelasticity (Mctigue, 1986), particularly when the heat flow in the matrix is dominated by the conductive heat transport. Often, heat flow in fracture network is dominated by the convective heat transport (Cheng et al., 2001), however, when the fracture is deformable, the dominant heat flow mechanism may change from convection to conductive transport when the fluid velocity is reduced a low value. Therefore, both convective and conductive heat transport mechanisms are considered herein. In addition to the coupling between stress, pore pressure, and temperature, the model considers the joint deformation characteristics in simulating the change of stress distribution and fracture permeability during injection and extraction operations in a fractured geothermal reservoir.

PORO-THERMOELASTIC DISPLACEMENT DISCONTINUITY METHOD (DDM)

The constitutive equations of the linear theory of poro-thermoelasticity are: (Mctigue, 1986)

$$\varepsilon_{ij} = \frac{1}{2G}\left[\sigma_{ij} - \frac{v}{1+v}\sigma_{kk}\delta_{ij}\right] + \frac{\alpha(1-2v)}{2G(1+v)}\delta_{ij}p + \frac{\alpha_s}{3}\delta_{ij}T \quad (1)$$

$$\zeta = \frac{\alpha(1-2v)}{2G(1+v)}\sigma_{kk} + \frac{\alpha^2(1-2v)^2(1+v_u)}{2G(1+v)(v_u-v)}p - \phi(\alpha_f - \alpha_s)T \quad (2)$$

where ε_{ij} and σ_{ij} are the change of strain and stress of the solid matrix, respectively, p and ζ are the change of pore pressure and pore volume respectively, T is the change of temperature and δ_{ij} is the Kronecker delta. The material constants are the bulk shear modulus G, Biot coefficient α, the drained and undrained Poisson's ratios v and v_u, Skempton's pore pressure coefficient B, and the volumetric thermal expansion coefficients of the solid matrix α_s and the pore fluid α_f. This version of the theory is suitable for when convective heat transport can be neglected in the porous matrix. Despite this simplifying assumption, the equations of the theory are generally not amenable to analytical solutions and require numerical modeling, particularly when considering fractures. The porothermoelastic extension of the elastic (Crouch and Starfied, 1981) and poroelastic (Curran and Carvalho, 1987) displacement discontinuity method has proven suitable for this purpose (Ghassemi and Zhang, 2004). The method has been developed based on Betti's reciprocal theory for poro-thermoelasticity.

Considering a thin fracture segment of length of $2a$ in a porous matrix of infinite extent (Figure 1), the pore pressure and stress induced by normal deformation ΔD_n, shear deformation ΔD_s, fluid injection Δq_{int} (the leakoff rate per fracture length), and heat flow rate $\Delta q_{h\text{-}int}$ (the interface heat flow rate per fracture

length) at a point (x, y) at time t are obtained by summing the fundamental solutions (Ghassemi and Zhang, 2006):

$$\Delta p(x,y,t) = p^{dn}(x,y,t)\,\Delta D_n + p^{ds}(x,y,t)\,\Delta D_s + p^{q}(x,y,t)\,\Delta q_{\text{int}} + p^{T}(x,y,t)\,\Delta q_{h-\text{int}} \tag{3}$$

$$\Delta \sigma_{ij}(x,y,t) = \sigma_{ij}^{dn}(x,y,t)\,\Delta D_n + \sigma_{ij}^{ds}(x,y,t)\,\Delta D_s + \sigma_{ij}^{q}(x,y,t)\,\Delta q_{\text{int}} + \sigma_{ij}^{T}(x,y,t)\,\Delta q_{h-\text{int}} \tag{4}$$

where the superscripts *dn*, *ds*, *q* and *T* denote normal displacement discontinuity source, shear displacement discontinuity source, fluid and heat source, respectively. The induced pressure and stress by constant unit fluid and heat source strengths (D_n, D_s, q_{int} and $q_{h\text{-}int}$) can be found in Carvalho (1990) and Zhang (2004). The induced temperature T at any point (x, y) and time is only dependent on the heat source $q_{h\text{-}int}$ and the effects of D_n, D_s, and q_{int} are neglected (Eq. 5)).

$$\Delta T(x,y,t) = T^{T}(x,y,t)\,\Delta q_{h-\text{int}} \tag{5}$$

For a multi-fracture system, there are interactions among the fracture segments. The induced temperature, pore pressure, normal and shear stress on the *ith* fracture segment by all fracture segments can be obtained by using the spatial and temporal superposition of the fundamental solutions:

$$\Delta \overset{i}{T}(t) = \sum_{j=1}^{m} \overset{ij}{T^{T}}(t)\,\Delta \overset{j}{q}_{h-\text{int}} \tag{6}$$

$$\Delta \overset{i}{p}(t) = \sum_{j=1}^{m} \overset{ij}{p^{dn}}(t)\,\Delta \overset{j}{D}_n + \sum_{j=1}^{m} \overset{ij}{p^{ds}}(t)\,\Delta \overset{j}{D}_s + \sum_{j=1}^{m} \overset{ij}{p^{q}}(t)\,\Delta \overset{j}{q}_{\text{int}} + \sum_{j=1}^{m} \overset{ij}{p^{T}}(t)\,\Delta \overset{j}{q}_{h-\text{int}} \tag{7}$$

$$\Delta \overset{i}{\sigma}_n(t) = \sum_{j=1}^{m} \overset{ij}{\sigma_n^{dn}}(t)\,\Delta \overset{j}{D}_n + \sum_{j=1}^{m} \overset{ij}{\sigma_n^{ds}}(t)\,\Delta \overset{j}{D}_s + \sum_{j=1}^{m} \overset{ij}{\sigma_n^{q}}(t)\,\Delta \overset{j}{q}_{\text{int}} + \sum_{j=1}^{m} \overset{ij}{\sigma_n^{T}}(t)\,\Delta \overset{j}{q}_{h-\text{int}} \tag{8}$$

$$\Delta \overset{i}{\sigma}_s(t) = \sum_{j=1}^{m} \overset{ij}{\sigma_s^{dn}}(t)\,\Delta \overset{j}{D}_n + \sum_{j=1}^{m} \overset{ij}{\sigma_s^{ds}}(t)\,\Delta \overset{j}{D}_s + \sum_{j=1}^{m} \overset{ij}{\sigma_s^{q}}(t)\,\Delta \overset{j}{q}_{\text{int}} + \sum_{j=1}^{m} \overset{ij}{\sigma_s^{T}}(t)\,\Delta \overset{j}{q}_{h-\text{int}} \tag{9}$$

where m denotes the total number of fracture segments, the over script *ij* denotes the influence of *jth* fracture segment on the *ith* fracture segment, and the over script *j* denotes the source strength of *jth* fracture segment.

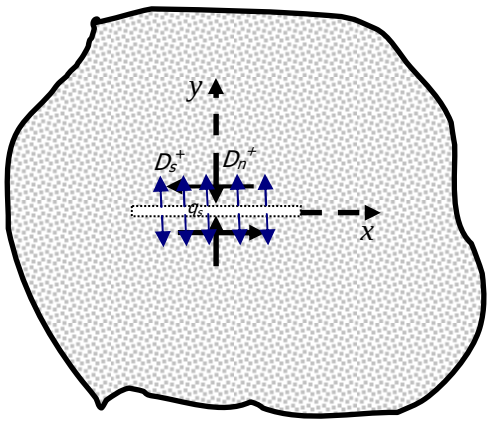

Figure 1: A thin line fracture in an infinite two-dimensional elastic porous medium, and the line fracture starts from (-a,0) and ends at (a,0).

To consider the time variation of the discontinuity strengths (ΔD_n, ΔD_s, Δq_{int} and $\Delta q_{h\text{-}int}$), we use a time marching scheme shown in Figure 2 to discretize the source strengths into step increments. Thus Eqs. (6)-(9) are rewritten as:

$$\Delta \overset{i}{T}(t) = \sum_{j=1}^{m} \overset{ij}{T^{T}}(t-\tau_\xi)\,\Delta \overset{j\xi}{q}_{h-\text{int}} + \sum_{h=0}^{\xi-1}\sum_{j=1}^{m} \overset{ij}{T^{T}}(t-\tau_h)\,\Delta \overset{jh}{q}_{h-\text{int}} \tag{10}$$

$$\Delta \overset{i}{p}(t) = \sum_{j=1}^{m} \overset{ij}{p^{dn}}(t-\tau_\xi)\,\Delta \overset{j\xi}{D}_n + \sum_{j=1}^{m} \overset{ij}{p^{ds}}(t-\tau_\xi)\,\Delta \overset{j\xi}{D}_s + \sum_{j=1}^{m} \overset{ij}{p^{q}}(t-\tau_\xi)\,\Delta \overset{j\xi}{q}_{\text{int}} + \sum_{j=1}^{m} \overset{ij}{p^{T}}(t-\tau_\xi)\,\Delta \overset{j\xi}{q}_{h-\text{int}} + \sum_{h=0}^{\xi-1}\sum_{j=1}^{m} \overset{ij}{p^{dn}}(t-\tau_h)\,\Delta \overset{jh}{D}_n + \sum_{h=0}^{\xi-1}\sum_{j=1}^{m} \overset{ij}{p^{ds}}(t-\tau_h)\,\Delta \overset{jh}{D}_s + \sum_{h=0}^{\xi-1}\sum_{j=1}^{m} \overset{ij}{p^{q}}(t-\tau_h)\,\Delta \overset{jh}{q}_{\text{int}} + \sum_{h=0}^{\xi-1}\sum_{j=1}^{m} \overset{ij}{p^{T}}(t-\tau_h)\,\Delta \overset{jh}{q}_{h-\text{int}} \tag{11}$$

$$\Delta \overset{i}{\sigma}_n(t) = \sum_{j=1}^{m} \overset{ij}{\sigma_n^{dn}}(t-\tau_\xi)\,\Delta \overset{j}{D}_n + \sum_{j=1}^{m} \overset{ij}{\sigma_n^{ds}}(t-\tau_\xi)\,\Delta \overset{j}{D}_s + \sum_{j=1}^{m} \overset{ij}{\sigma_n^{q}}(t-\tau_\xi)\,\Delta \overset{j}{q}_{\text{int}} + \sum_{j=1}^{m} \overset{ij}{\sigma_n^{T}}(t-\tau_\xi)\,\Delta \overset{j}{q}_{h-\text{int}} + \sum_{h=0}^{\xi-1}\sum_{j=1}^{m} \overset{ij}{\sigma_n^{dn}}(t-\tau_h)\,\Delta \overset{jh}{D}_n + \sum_{h=0}^{\xi-1}\sum_{j=1}^{m} \overset{ij}{\sigma_n^{ds}}(t-\tau_h)\,\Delta \overset{jh}{D}_s + \sum_{h=0}^{\xi-1}\sum_{j=1}^{m} \overset{ij}{\sigma_n^{q}}(t-\tau_h)\,\Delta \overset{jh}{q}_{\text{int}} + \sum_{h=0}^{\xi-1}\sum_{j=1}^{m} \overset{ij}{\sigma_n^{T}}(t-\tau_h)\,\Delta \overset{jh}{q}_{h-\text{int}} \tag{12}$$

$$\Delta\overset{i}{\sigma}_s(t)=\sum_{j=1}^{m}\overset{ij}{\sigma}_s^{dn}(t-\tau_\xi)\Delta\overset{j\xi}{D}_n$$
$$+\sum_{j=1}^{m}\overset{ij}{\sigma}_s^{ds}(t-\tau_\xi)\Delta\overset{j\xi}{D}_s+\sum_{j=1}^{m}\overset{ij}{\sigma}_s^{q}(t-\tau_\xi)\Delta\overset{j\xi}{q}_{\text{int}}$$
$$+\sum_{j=1}^{m}\overset{ij}{\sigma}_s^{T}(t-\tau_\xi)\Delta\overset{j\xi}{q}_{h-\text{int}}+\sum_{h=0}^{\xi-1}\sum_{j=1}^{m}\overset{ij}{\sigma}_s^{dn}(t-\tau_h)\Delta\overset{jh}{D}_n \quad (13)$$
$$+\sum_{h=0}^{\xi-1}\sum_{j=1}^{m}\overset{ij}{\sigma}_s^{ds}(t-\tau_h)\Delta\overset{jh}{D}_s+\sum_{h=0}^{\xi-1}\sum_{j=1}^{m}\overset{ij}{\sigma}_s^{q}(t-\tau_h)\Delta\overset{jh}{q}_{\text{int}}$$
$$+\sum_{h=0}^{\xi-1}\sum_{j=1}^{m}\overset{ij}{\sigma}_s^{T}(t-\tau_h)\Delta\overset{jh}{q}_{h-\text{int}}$$

where $\Delta\overset{j\xi}{D}_n$, $\Delta\overset{j\xi}{D}_s$, $\Delta\overset{j\xi}{q}_{\text{int}}$ and $\Delta\overset{j\xi}{q}_{h-\text{int}}$ are the source strength increments for the *jth* fracture segment at the current time step, ξ; $\Delta\overset{jh}{D}_n$, $\Delta\overset{jh}{D}_s$, $\Delta\overset{jh}{q}_{\text{int}}$ and $\Delta\overset{jh}{q}_{h-\text{int}}$ are the previous source strength increments of for the *jth* fracture segment at time step *h*, which indexed from 1 to ξ-1.

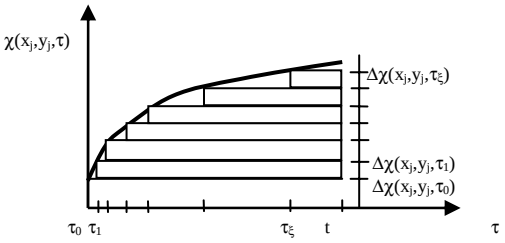

Figure 2: Time marching scheme, χ represents D_n, D_s or q_{int} (after Curran & Carvalho, 1987).

FLUID TRANSPORT IN FRACTURES

The aperture of a real fracture varies in space, and the fluid flow inside can also very complicated due to the rough surfaces. But Darcy's law is still considered valid and the rough fracture can be represented by a fracture with the average fracture aperture (Witherspoon et al. 1980). The coupled fluid flow equation (Eq. (14)) for a fracture-matrix system can be written as: (Tao et al. 2010):

$$\frac{k_f w_f}{\mu}\nabla^2 p=2aw_f c_f\frac{\partial p}{\partial t}-2a\frac{\partial D_n}{\partial t}+2aq_{\text{int}}+q_s \quad (14)$$

where k_f is the fracture permeability (k_f=w_f^2/12), w_f is the fracture aperture, μ is the fluid viscosity, c_f is the fluid compressibility, and q_s is the source term (injection or production).

HEAT TRANSPORT IN FRACTURES

The energy conservation equation (Eq. (15)) in a fracture-matrix system is built by considering the rate of internal energy, Δ*U*, the heat flow rate at the interface between fracture and matrix, $Q_{h\text{-}int}$, rate of energy change by conductive transport within the fracture, ΔE_d, and the energy change rate by convective transport in fracture, ΔE_v.

$$\Delta U=\Delta E_d+\Delta E_v+Q_{h-\text{int}} \quad (15)$$

For a fracture segment of length of 2a with an aperture, w_f , in a fracture-matrix system of unit thickness (Figure 3), the rate of internal energy change is only resulted from the temperature change (Eq. (16)) if the influence of the change of fracture aperture and fluid density are negligible.

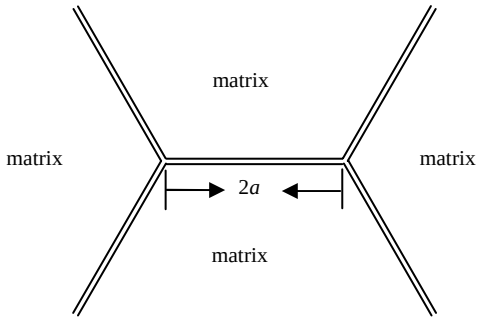

Figure 3: Illustration of a fracture segment in a fracture-matrix system.

$$\Delta U=2a\,w_f\rho_w c_w\frac{\partial T}{\partial t} \quad (16)$$

where ρ_w and c_w are the fluid density and heat capacity, respectively. The energy change rate by conductive transport in the fracture segment is given by the net conductive heat flow into the fracture segment through the connections to other fractures.

$$\Delta E_d=-\nabla\cdot Q_{heat} \quad (17)$$

where Q_{heat} is the conductive heat flow rate in fractures and given by the Fourier's law.

$$Q_{heat}=-k_T w_f\nabla T \quad (18)$$

where k_T is the thermal conductivity in fluid and the cross section area of heat flow is w_f as the thickness is unit. Substituting Eq. (18) for Q_{heat} in Eq. (17) yields:

$$\Delta E_d=k_T w_f\nabla^2 T \quad (19)$$

The heat flow into the fracture segment by convective transport is given by:

$$\Delta E_v=-2a\,\rho_w c_w q_f\nabla T \quad (20)$$

where q_f is the flow rate in the fracture segment. The interface heat flow rate is:

$$Q_{h-\text{int}}=-2aq_{h-\text{int}} \quad (21)$$

Combining Eqs. (15)-(21) yields the energy conservation equation (Eq. (22)) in a fracture-matrix system.

$$2a\,w_f\rho_w c_w\frac{\partial T}{\partial t}=k_T w_f\nabla^2 T-2a\,\rho_w c_w q_f\nabla T$$
$$-2aq_{h-\text{int}} \quad (22)$$

FRACTURE DEFORMATION

The change of normal and shear stress acting on the fracture segment induces normal and shear deformation. To simulate this response of a rough fracture (Figure 4), the Barton-Bandis (1983) joint deformation model is applied in this study. In this model, the normal stress is a hyperbolic function of the normal closure.

$$\sigma_n^{'} = \frac{K_{ni} D_n}{1 - D_n / D_{n\max}} \tag{23}$$

where σ_n' is the effective normal stress. But when the fracture deformation is small, the change of stress with the fracture closure can be approximated as a linear relation:

$$\Delta\sigma_n^{'} = -K_n \, \Delta D_n \tag{24}$$

For the hyperbolic model, the normal stiffness (K_n) is a function of D_n or σ'_n:

$$K_n = \frac{\partial \sigma_n^{'}}{\partial D_n} = \frac{K_{ni}}{\left(1 - D_n / D_{n\max}\right)^2} \tag{25}$$

or

$$K_n = \frac{K_{ni}}{\left[1 - \sigma_n^{'} / \left(K_{ni} D_{n\max} + \sigma_n^{'}\right)\right]^2} \tag{26}$$

where K_{ni} is the initial normal stiffness and D_{nmax} is the maximum fracture closure. The change of shear stress has a linear relationship with the change of shear displacement before yielding:

$$\Delta\sigma_s = K_s \, \Delta D_s \tag{27}$$

where K_s is the shear stiffness. The fracture slips when the shear stress exceeds the shear strength (σ_c) of the fracture. We use an approximate linear relation for the aperture increase ($\Delta D_{n\text{-dilation}}$) in response to shear movement.

$$\Delta D_{n-dilation} = -\Delta D_s \tan\phi_d \tag{28}$$

where ϕ_d is the dilation angle. Eq. (24) is rewritten when the shear dilation is considered and the effective stress σ_n' is expressed by total stress and fluid pressure:

$$\Delta\sigma_n + \Delta p = -K_n \left(\Delta D_n + \Delta D_s \tan\phi_d\right) \tag{29}$$

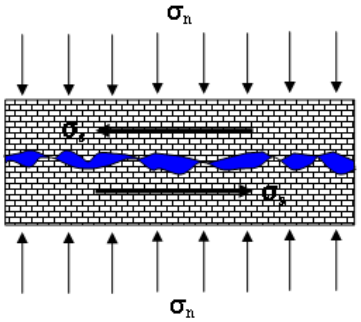

Figure 4: A fluid filled fracture subject to normal and shear stress.

SOLUTION METHOD

The fluid flow equation (Eq. (14)) for a given fracture network is discretized in space and time using an implicit finite difference method. For the *ith* fracture segment at the time step, ξ, the discretized fluid diffusivity equation is:

$$\sum_{j=1}^{m} \overset{ij}{C}_p \, \overset{j}{p}(t) - 2a\Delta \overset{i\xi}{D}_n + 2a\Delta \overset{i\xi}{q}_{\text{int}} = 2a w_f c_f \, \overset{i}{p}(\tau_\xi) - 2a\sum_{h=0}^{\xi-1} \Delta \overset{ih}{q}_{\text{int}} - \sum_{h=0}^{\xi} \overset{ih}{q}_s \tag{30}$$

where $\overset{ij}{C}_p$ is the fluid coefficient matrix (Tao, 2010), which represents fluid diffusion in the fracture network. Similarly, the heat transport equation (Eq. (22)) can be discretized in space and time for a given fracture network.

$$\sum_{j=1}^{m} \overset{ij}{C}_{ht} \, \overset{j}{T}(t) + 2a\Delta \overset{i\xi}{q}_{h-\text{int}} = 2a \, w_f \rho_w c_w \, \overset{i}{T}(\tau_\xi) \tag{31}$$

where $\overset{ij}{C}_{ht}$ is the coefficient matrix for heat transport in fractures representing heat transport in the fracture network. The $\overset{ij}{C}_{ht}$ is dependent on the fluid flow rate, q_f, in fractures. Consequently, Eq. (31) is coupled with the fluid flow rate in the fractures.

After building sets of linear equations from Eq. (10) and Eq. (31), the temperature distribution and interface heat flow rate at every fracture segment can be solved for given fluid flow rate in fractures. Combining Eqs. (11)-(13), (27), (29) and (30), the fluid pressure, normal and shear fracture deformation, and interface flow rate can be solved for given interface heat flow rate. The above two solution steps are coupled, therefore iterations are needed to solve for the distribution of temperature and fluid pressure, and fracture deformation.

MODEL APPLICATION

Consider two sets of fractures with angle of 60° (Figure 5) in Westerly Granite with a unit thickness

(1 m). There are two wells connected with the fracture network (Figure 5). One is an injection well and the other is a production well. Both wells have the same flow rate of 1×10^{-4} m^3/sec. To isolate the poro-thermoelastic phenomena, the in-situ stress field, and reservoir pressure before production are assumed to be isotropic and homogeneous, and set as 30 MPa and 27 MPa, respectively. The initial reservoir temperature is 420 K and the injection water has a constant temperature of 300 K. In the numerical solution, this condition is implemented by instantly setting the temperature of the fracture element intersected by the injection well to a temperature of 300 K at the start of the injection. The two joint parameters that characterize the normal deformation of fracture namely, the initial normal stiffness and the maximum closure are set to 0.5 GPa/m and 0.8mm, respectively. The nonlinear relationship between the effective normal stress under compression and the fracture closure is shown in Figure 6. The fracture aperture at the initial condition (zero effective normal stress) is assumed as 3.0 mm. The fracture aperture under the initial in-situ stress but prior to injection/production is assumed as 1.0 mm for all fractures. Other input parameters are listed in

Table 1 and the parameters for Westerly Granite are extracted from Mctigue (1990).

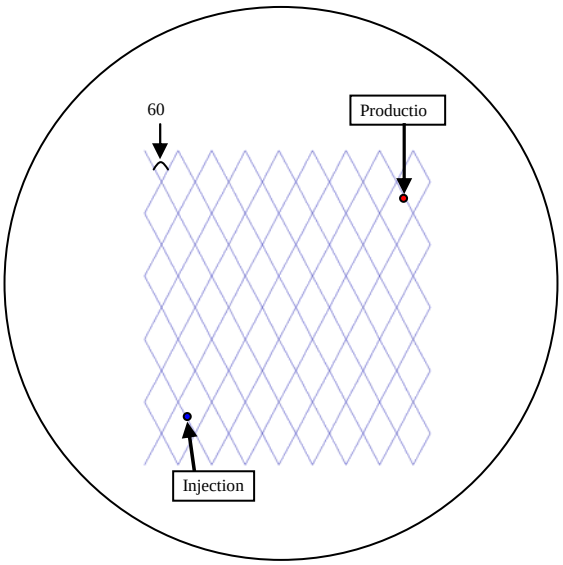

Figure 5: A regular fracture network with a injection well and a production well (fracture spacing of 203.77 m*).*

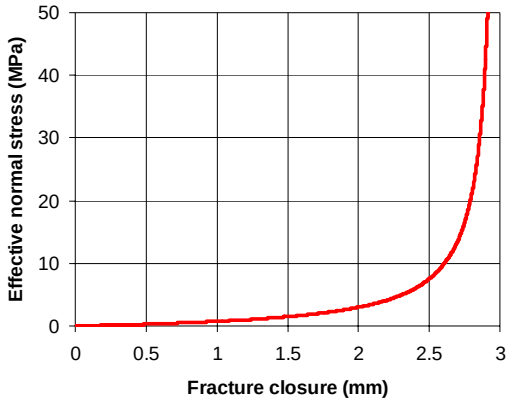

Figure 6: Nonlinear fracture normal deformation.

Table 1: Input parameters.

Area of fracture network (m^2)	2000×2000
Shear modulus G (GPa)	15
Possoin's ratio υ	0.25
Undrained Possoin's ratio υ_u	0.33
Matrix permeability (m^2)	4×10^{-19}
Matrix porosity ϕ	0.01
Biot's coefficient α	0.44
Fluid viscosity μ (cp)	3.547×10^{-4}
Fluid compressibility (MPa^{-1})	4.2×10^{-4}
Thermal expansion coefficient of solid α_s (K^{-1})	2.4×10^{-5}
Thermal expansion coefficient of solid α_f (K^{-1})	2.1×10^{-5}
Thermal diffusivity of intact porous rock c^T (m^2/s)	$1.1\text{x}10^{-6}$
Fluid density ρ_w (Kg/m^3)	$1\text{ x}10^3$
Heat capacity of fluid c_w ($J\ kg^{-1}\ K^{-1}$)	4200
Thermal conductivity of fluid k_T ($J\ s^{-1}\ m^{-1}\ K^{-1}$)	0.6

Figure 7 shows the temperature distribution within the fractured reservoir after one year of cold water injection. It can be seen that the temperature around the injection well is reduced and the temperature of fractures far from the injection well is not affected. The pressure in the whole fracture network is reduced to be below the initial reservoir pressure (27 MPa) due to the cooling effect on the matrix and the fracture aperture (Figure 8). For isothermal injection, the pressure at the production well increases with time and then reaches the steady state. When injecting cooler water, the pressure at the injection well begins to increase after initially decreasing because of the cooling effect, and then continuously drops as the cooling effect. The pressure at the production well drops with time, and continues dropping as injection proceeds and the cooling effect reduces the pressure. The pressure responses can be explained by considering the fracture aperture history

((Figure 10). The aperture at the injection well, where the cooling effect is much more than the hydraulic effect, (compare with isothermal injection) is enhanced.

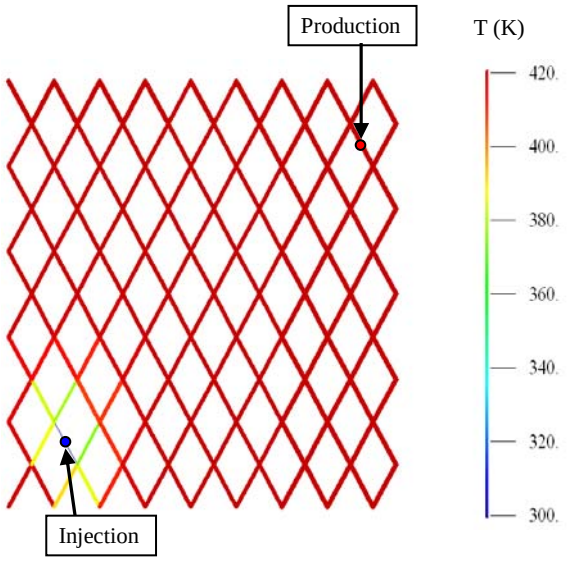

Figure 7: Temperature distribution after one year of injection and production.

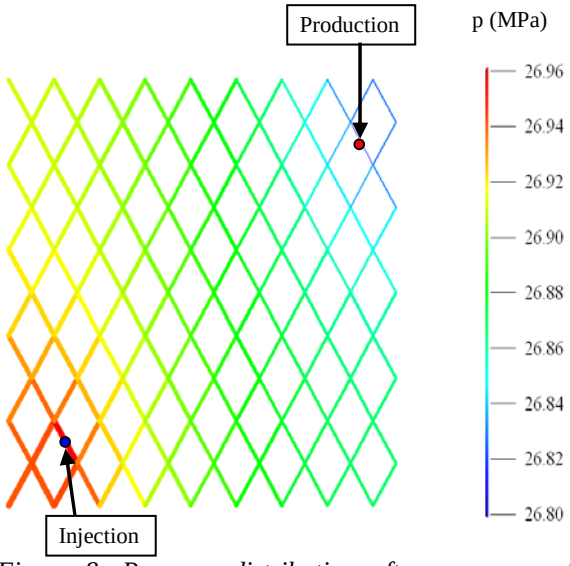

Figure 8: Pressure distribution after one year of injection and production.

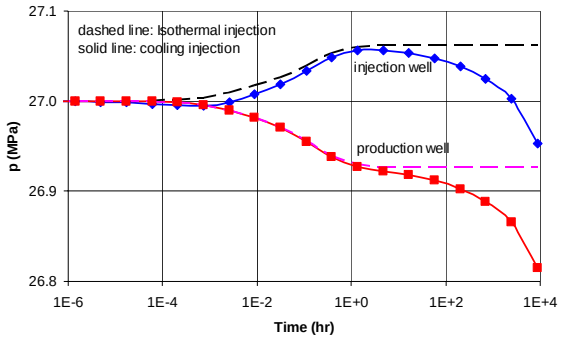

Figure 9: The transient pressure at injection well and production.

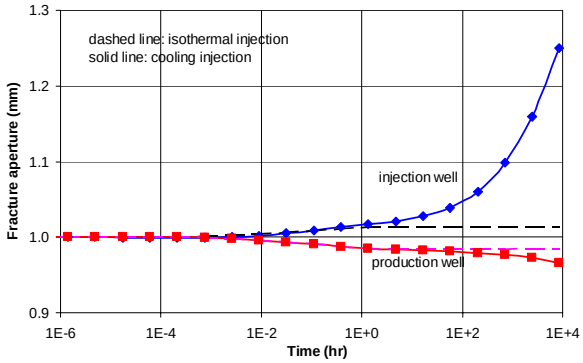

Figure 10: Fracture aperture at the injection well and production well changes with time.

CONCLUSIONS

A fully coupled model is developed to simulate a non-isothermal compressible single-phase fluid flow in fractured porous media by combining the poro-thermoelastic DDM, the Barton-Bandis nonlinear joint deformation model, and a finite difference method solving the fluid and heat transport in a regular fracture network. Both conductive and convective heat transport in fractures are considered in the model. But only conductive heat transport is considered in matrix and the convective heat transport is neglected as the fluid flow rate is much slower than that in fractures for low permeable rock, e.g. Westerly Granite.

The model is applied to simulate the cooler water injection and heat production in a fractured poro-thermoelastic reservoir. The application shows that the cooling effect reduces the pressure of whole fracture network, and enhances the fracture aperture near the cooling injection well.

ACKNOWLEDGEMENTS

This project was supported by the U.S. Department of Energy Office of Energy Efficiency and Renewable Energy under Cooperative Agreement DE-FG36-06GO16059. This support does not constitute an endorsement by the U.S. Department of Energy of the views expressed in this publication.

REFERENCES

Bandis, S.C., Lumsden, A.C. and Barton, N.R., 1983. Fundamentals of Rock Joint Deformation. *International Journal of Rock Mechanics and Mining Sciences & Geomechanics Abstracts* **20** (6): 249-268.

Cheng A.H.-D., Ghassemi A. and Detournay E., 2001. Integral Equation Solution of Heat Extraction From a Fracture in Hot Dry Rock. *International Journal for Numerical and Analytical Methods in Geomechanics* **25**(13), 1327-1338.

Curran, J.H., and Carvalho, J.L. 1987."A displacement discontinuity model for fluid-saturated porous media."Proc., 6th Congress of the ISRM, Vol.1, Montreal,73–78.

Ghassemi, A., Nygren A. and Cheng A.H.-D., 2008. Effect of Heat Extraction on Fracture Aperture: A Poro-Theromoelastic Analysis. *Geothermics* **37**(5), 525-539.

Ghassemi A. and Zhang Q., 2004. A Transient Fictitious Stress Boundary Element Method for Porothermoelastic Media. *Engineering Analysis with Boundary Elements* **28**(11), 1363–1373.

McTigue, D.F., 1986. Thermoelastic response of fluid-saturated porous rock. *Journal of Geophysical Research* **91**(B9), 9533–9542.

McTigue, D.F., 1990. Flow to a heated borehole in porous, thermoelastic rock: Analysis. *Water Resources Research* **26**(8), 1763-1774.

Tao Q., C.A. Ehlig-Economides and A. Ghassemi. A Fully Coupled Method to Model Fracture Permeability Change in Naturally Fractured Reservoirs. (submitted to *International Journal of Rock Mechanics and Mining Sciences*)

Tao Q., 2010. Numerical Modeling of Fracture Permeability Change in Naturally Fractured Reservoirs Using a Fully Coupled Displacement Discontinuity Method. Ph.D. Dissertation, Texas A&M University, College Station, Texas.

Witherspoon, P.A., Wang, J.S.Y., Iwai, K., and Gale, J. E., 1980. Validity of Cubic Law for Fluid Flow in a Deformable Rock Fracture. *Water Resources Research* **16**, 1016-1024.

Ghassemi, A., and Zhang, Q., 2006. Poro-thermoelastic response of a stationary crack using the displacement discontinuity method. *ASCE Journal of Engineering Mechanics* **132**(1), 26-33.

Zhang, Q., 2004. A Boundary Element Method for Thermo-Poroelasticity With Applications in Rock Mechanics. Master's thesis, Univ. of North Dakota, Grand Forks, North Dakota.